Research Article

Optimization of the critical overlap length of hudraulic distributors regarding cavitation inception

Mahamadou Adama Maiga[1] · Olivier Coutier-Delgosha[1,2] · Daniel Buisine[1]

Received: 23 November 2020 / Accepted: 4 August 2021
Published online: 07 September 2021

Abstract
The present paper is focused on the optimization of the overlap length in various types of distributors in hydraulic systems. It has been shown that this length has a strong influence on cavitation in rotating distributors, so its optimization would be beneficial to reduce the detrimental effects of cavitation, such as noise, vibrations, and instabilities. The objective of the present study is to generalize the modelling of the overlap length to different types of distributors and to determine the critical length at cavitation inception. The results show that the pressure losses in rotating distributors and in other types of distributors are similar, including the slide-valves that are the vast majority of distributors in hydraulic systems. It is confirmed that the overlap length has a stronger influence on the cavitation development than the distributor rotation speed. A critical overlap length of 0.071 mm is obtained, below which no significant development of cavitation is obtained, at all rotation speeds.

Article Highlights

- The pressure losses in a rotating distributor and in a slide-valve can be expressed similarly.
- The overlap length has a large influence on the cavitation development, much larger than the rotation speed.
- A critical overlap length of 0.071 mm was obtained, below which there is almost no cavitation, for any rotation speed.

Keywords Hydraulic distributors · Cavitation · Modeling · Optimization · Overlap length

Abbreviations

i, j	Index used to denote a bubble number [–]
N_b	Total number of bubbles [–]
t	Time [s]
Δt	Time step [s]
R_i	Radius of bubble i [m]
R_{0i}	Initial radius of bubble i radius [m]
R_{moy}	Average radius [m]
R_{cs_i}	Critical radius of bubble i [m]
$\dot{R}_i$	Velocity normal to the interface of bubble i [m/s]
$\ddot{R}_i$	Acceleration at the interface of bubble i [m/s^2]
$q_i = 4\pi R_i^2 \dot{R}_i$	Flow rate through the interface of bubble i [m^3/s]

✉ Mahamadou Adama Maiga, mahamadoumaiga@yahoo.fr | [1]UMR 9014 - LMFL - Laboratoire de Mécanique des Fluides de Lille - Kampé de Fériet, Univ. Lille, CNRS, ONERA, Arts et Metiers Institute of Technology, Centrale Lille, 59000 Lille, France. [2]Kevin T. Crofton Department of Aerospace & Ocean Engineering, Virginia Tech, Blacksburg, VA 24060, USA.

$\dot{q}_i = \frac{\partial q_i}{\partial t} = 4\pi\left(2R_i\dot{R}_i^2 + R_i^2\ddot{R}_i\right)$	Time derivative of q_i [m^3/s^2]
D_{ij}	Distance between the centers of bubbles i and j [m]
D_0	$D_{ij}/\left(R_{0i} + R_{0j}\right)$ [–]
T	Surface tension [N/m]
μ_L	Dynamic viscosity of the liquid [pa.s]
ρ_L	Density of the liquid [kg/m^3]
$p_{ex}(t)$	Ambient pressure [pa]
p_i	Pressure in the liquid at the interface of bubble i [pa]
p_0	Atmospheric pressure [pa]
p_v	Vapour pressure [pa]
p_{g_i}	Gas pressure in bubble i [pa]
p_{cs_i}	Critical pressure [pa]
γ	Polytropitic exponent [–]
φ	Angular position of the distributor [rad]
X_{dis}	Abscissa of M, located at the periphery of the distributor [m]
X_{clo}	Distributor travel for $X_{dis} < 0$ [m]
X_{ope}	Distributor travel for $X_{dis} > 0$ [m]
X_{ove}	Overlap length [m]
H_{gap}	Gap length [m]
H_{hei}	Chamber height [m]
L_{dis}	Distributor length in the z direction [m]
V_{ch}	Chamber volume [m^3]
R_{dis}	Radius of the rotating distributor [m]
R_{cra}	Crank shaft radius [m]
S_{pis}	Piston section [m^2]
Q_{dis}	Distributor flow rate [m^3/s]
Q_{pis}	Piston flow rate [m^3/s]
ω	Angular velocity [rad/s]
Ω	Rotational speed [rpm]
V_{dis}	Slide-valve speed [rpm]
p_c	Chamber pressure [pa]
p_{pump}	Pressure at the pump outlet [pa]
δp_{clo}	Pressure drop if the distributor is closed [pa]
δp_{ope}	Pressure drop if the distributor is open [pa]
δp	Pressure drop [pa]
Re	Reynolds number [–]
We	Weber number [–]
σ	Cavitation number [–]

1 Introduction

The optimization of engine parts, in terms of performance, lifetime, weight and volume minimization, remains a permanent challenge for designers, in various areas like aerospace and car engineering. In that process, the modelling has become a crucial step to optimize the shape and dimensions while taking into account the operating conditions.

Many previous studies [1–5] show that some minor geometrical details (local shape, surface roughness, coating…) in engine parts strongly influence the onset and development of certain physical phenomena like cavitation, for various types of systems such as rotating machinery. In addition, these studies confirm that the modelling of the influence of these details on the engine operation can help in the optimization process.

For example, a hydro-elastic model for the design and optimization of a flexible composite marine propeller is presented in [6]. The aim is to tailor the laminate to control the deformed shape of the blade and consequently the developed thrust and, thus, to minimize the fuel consumption. A 1.25% reduction of the consumption could be obtained, which leads to a decrease of 4.7% in the cruising speed condition. In [7], an experimental study of a fan included in a vehicle cooling system was performed: the objective was to analyse the effect of the position of the engine block, downstream from the fan, on the flow. The authors show that the fan performance is considerably influenced by the blockage induced by the engine block, as the mean flow velocity is especially dependant on the distance between the fan and the engine. In an other study on the micro hydro application of a turbine, for energy recovery schemes where the available head does not exceed 2 m, [8] presents a wide range of geometrical optimization steps carried out on a propeller runner, whose blades have been designed using the free vortex theory, and operating with a gross head from 1.5 to 2 m and discharge of approximately 75 l/s. The results show that the performance of the runner was very sensitive to changes of the exit tip angle, and the optimization study is very encouraging from the perspectives of micro hydro application. Also, in a study on the experimental and numerical investigation of the effect of surface roughness of casing and adhesive coating on the efficiency of centrifugal pump, [9] shows that, for different mass flow rates values, the surface roughness of the casing has a considerable effect on pump performance. In the same vein, [10] proposes a novel multi-objective evolution algorithm for the design of tidal turbine blade airfoil, to overcome the adverse effects of cavitation and roughness. Numerical simulations and experimental results show that the optimized airfoil enjoys a better aerodynamic performance than the

original ones, in terms of cavitation inhibition. Previously already, in a study applied to the design of a CPP propeller at different pitch settings, with the aim of reducing cavitation and the radiated noise, [11] showed the capability of a method based on the coupling between a multi-objective optimization algorithm and a panel code, to assess propeller functioning characteristics. The study shows that the method represents a very useful tool for the designer. In the case of a 3-way reversing valve, [12] used numerical simulations combined with a parametric study to obtain an optimal shape design that minimizes the cavitation effects at the bottom plug level. In [13], embarked acoustic measurements enabled to show that the noise level perceived in the cockpit of vehicles is strongly linked to the vibrations of the automatic gear box (BVA), especially coming from the moving bodies of the oil pump TA96. The study shows that the vibrations of the gear box are mostly due to cavitation, and a slight modification of the discharge chamber geometry of the oil pump leads to a significant decrease of the vibrations and thus the noise.

In another investigation on the influence of the rotating distributor geometry on cavitation inception in a hydraulic system, [14] also showed that some geometrical details have a strong influence on cavitation, and that the optimization of these details in engines, taking into account cavitation, would be an appropriate solution to reduce its effects. The study highlights particularly a critical overlap length above which cavitation is strongly influenced. However, this previous study was focused on a single rotating distributor and the critical overlap length is determined for a single rotational speed, which is assumed to be constant.

The distributor is a crucial part in hydraulic systems such as hoist loads, hydraulic shovels, power steering, and ventricular assistance devices, to name only a few. It can be of different types like slide-valve, rotating, valve etc. The distributor's role is to close, open, or deflect the flow in hydraulic systems, downstream from a pump, with an automatic, semi-automatic, or manual control. During the opening phase, a large pressure drop is obtained in the receiver close to the distributor, which generates cavitation.

The present study is the continuation of the previous work from the same authors [14]. The present paper generalizes the modelling of the overlap length to different types of distributors in order to determine the critical overlap length at cavitation inception. For that purpose, it is showed that the pressure losses in all types of distributors are similar to the losses in a rotating one. It is especially important for slide-valves, which represent the vast majority of distributors used in hydraulic systems. Thus, the next part of the study is focused on rotating distributors: for different rotational speeds, the critical overlap length is calculated and expressed as a function of the flow conditions (Reynolds and Weber numbers) to determine the global minimum value of the critical length.

This work is divided into two parts. First, the multi-bubble model for cavitation is presented, as well as the mechanism of pressure drop in the rotating and slide-valve distributors, and the hydraulic system already used in [14]. The second part of the paper is dedicated to the results and the discussion.

2 Theoretical formulation

2.1 Multi-bubble model

Previous studies [15, 16] show that the interactions between bubbles are significant at the early stage of cavitation inception. To account for these phenomena, a multi-bubble model was developed on the basis of the Rayleigh-Plesset equation, with additional terms to account for the bubble/bubble interactions [17, 18]. Here, the interactions between N_b bubbles are taken into account. The expansion rate of bubble i can be written as follows, i varying between 1 and N_b:

$$\dot{q}_i = \frac{1}{8\pi}\frac{q_i^2}{R_i^3} - \frac{4\mu_L}{\rho_L}\frac{q_i}{R_i^2} + \frac{4\pi R_i}{\rho_L}\left(p_{g_i} + p_v - p_{ex}(t)\right) - \frac{8\pi T}{\rho_L} - \sum_{j=1, j\neq i}^{N_b}\frac{R_i}{D_{ij}}\dot{q}_j \tag{1}$$

With $q_i = 4\pi R_i^2 \dot{R}_i$ the flow rate across the interface of bubble i, $\dot{R}_i$ the velocity normal to the interface, $\ddot{R}_i$ the interface acceleration, $\dot{q}_i = \frac{\partial q_i}{\partial t} = 4\pi\left(2R_i\dot{R}_i^2 + R_i^2\ddot{R}_i\right)$, T the surface tension, μ_L the liquid dynamic viscosity, ρ_L the liquid density, p_i the pressure in the liquid at the bubble interface and D_{ij} the distance between the centers of bubbles i and j. The pressure inside the bubble equals the sum of the vapour pressure p_v and the gas pressure p_{g_i} modelled by the barotropic Laplace law:

$$p_{g_i} = \left(p_0 + \frac{2\sigma}{R_{0i}} - p_v\right)\left(\frac{R_{0i}}{R_i}\right)^{3\gamma} \tag{2}$$

where R_{0i} is the bubble initial radius, γ the polytropic exponent, p_0 the atmospheric pressure and $p_{ex}(t)$ the ambient pressure.

2.2 Evaluation of the pressure drop in distributors

A distributor enables to open, shut down, or deflect the flow in hydraulic systems. In the closed position, the overlap has the effect of reducing the leaks and maintaining the pressure in the hydraulic system. In the gap between the distributor and the receiver casing, the pressure drop is of the Poiseuille

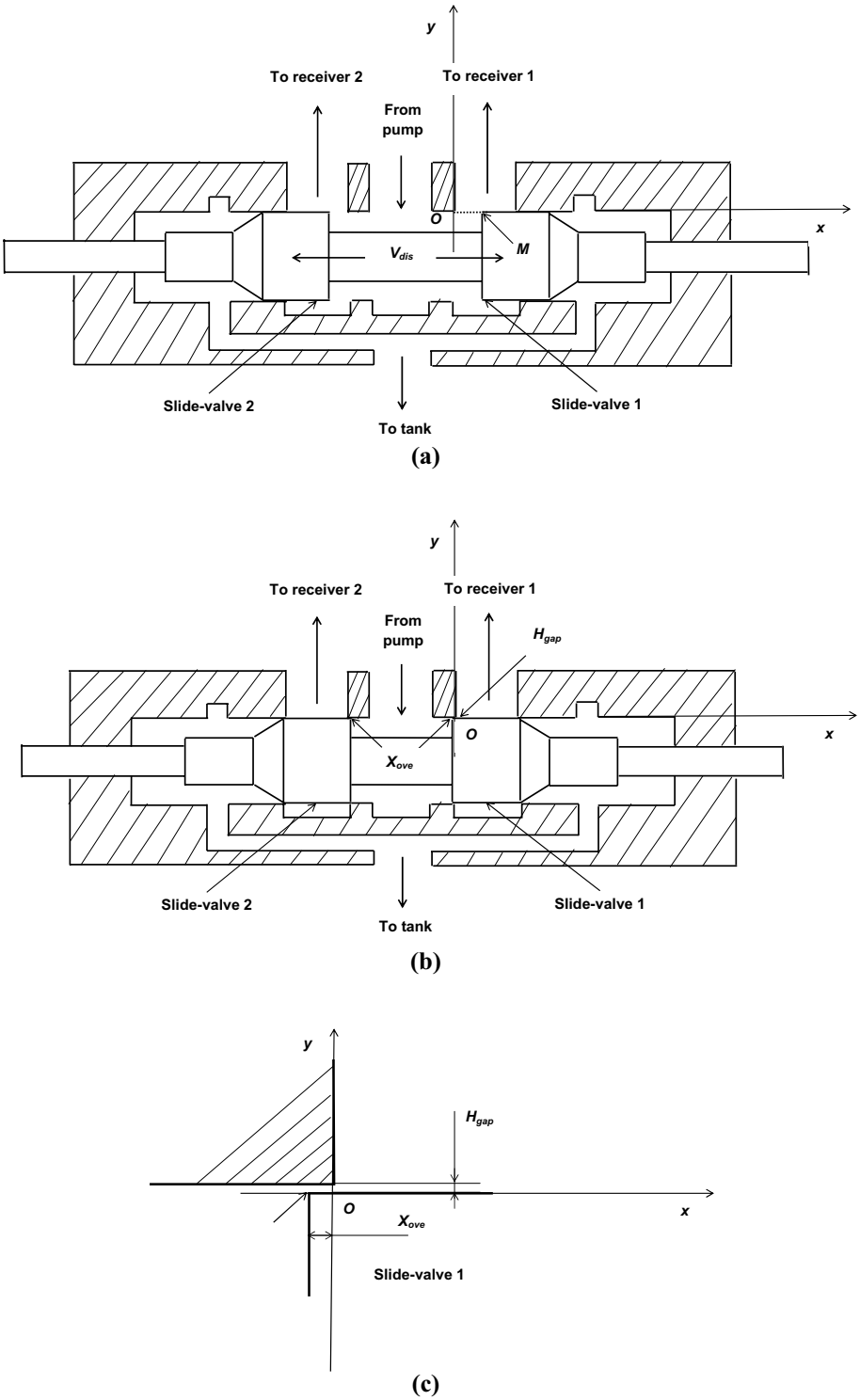

Fig. 1 Scheme of the slide-valve system **a** distributor opened, **b** distributor closed, **c** zoom at the overlap in case b

type. When the distributor is opening, thus delivering the fluid coming from the pump to the receiver, the pressure drop becomes singular and equal to the kinetic energy of the fluid coming from the distributor to the receiver.

The two examples of slide-valve and rotating distributors are presented hereafter. The slide-valve distributor is used in most of the hydraulic systems. In these two different types of distributors shown in Figs. 1 and 2, respectively, the opening, closing or adjustment of the circulation channel is made through a rectilinear displacement and a rotation, respectively. Figures 1a and 2a show the opening phase, while Figs. 1b, c, 2b, c represent the closed positions.

If the pressure in the receiver is assumed to be uniform, the flow rate and the pressure drop in the passage

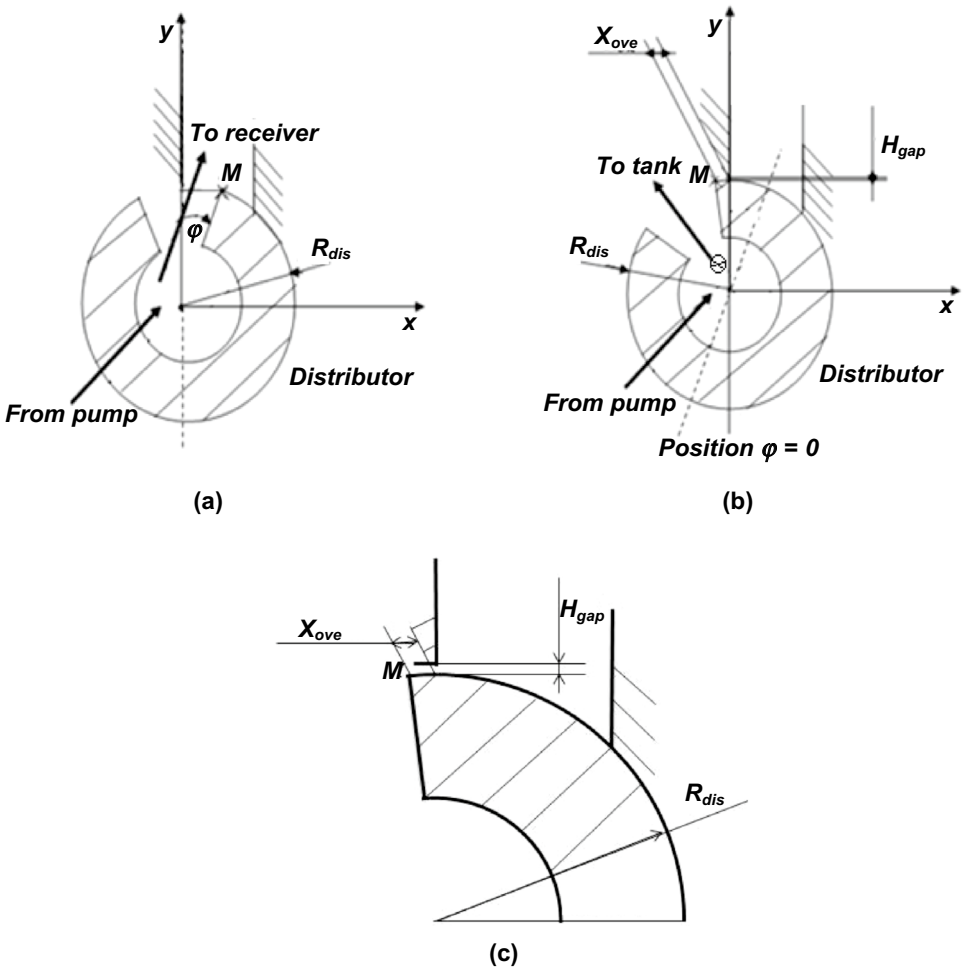

Fig. 2 Scheme of the rotating system **a** distributor opened, **b** distributor closed, **c** zoom at the overlap in case b

between the distributor and the receiver enable to determine the receiver pressure. The knowledge of the distributor motion is required to determine the flow rate. For the motion, as shown in Figs. 1 and 2, one considers the points *O* and *M* where *O* is located at the distributor's axis and *M* at its periphery. In addition, the rotational and slide-valve speeds are assumed to be steady during the simulation.

For the slide-valve, the distributor position, i.e. the the abscissa X_{dis} of *M*, can be derived from the uniform velocity V_{dis} and the overlap length X_{ove}, as shown in Fig. 1:

$$X_{dis} = V_{dis}t - X_{ove}, \tag{3}$$

For the rotating distributor, the abscissa X_{dis} of *M* is derived from the angle $\varphi = \left(\vec{y}, \overrightarrow{OM}\right)$ (see Fig. 2):

$$X_{dis} = R_{dis}\sin\varphi - X_{ove} = R_{dis}\sin\omega t - X_{ove}, \tag{4}$$

where R_{dis} is the radius of the distributor, $\omega = 2\pi\Omega/60$ its angular velocity and Ω its rotational speed in rotations per minute.

For calculations, X_{clo} is defined as the distributor motion for $X_{dis} < 0$ (when it is closed) and X_{ope} is the motion when $X_{dis} > 0$ (when it is opened):

$$X_{clo} = \frac{-X_{dis} + |X_{dis}|}{2}, \text{ is equal to } -X_{dis} \text{ when } X_{dis} < 0 \text{ and towhen } X_{dis} > 0, \tag{5}$$

$$X_{ope} = \frac{X_{dis} + |X_{dis}|}{2}, \text{ is equal to } X_{dis} \text{ when } X_{dis} < 0 \text{ and towhen } X_{dis} > 0, \tag{6}$$

For the rotating distributor, all assumptions made in [14] are used here. In addition, it is assumed that the slide-valve and rotating distributors have the same width L_{dis} in the z direction.

In the closed position, the pressure drop in the distributors is given by the Poiseuille formula:

$$\frac{X_{clo}}{L_{dis}} Q_{dis} = \frac{H_{gap}^3}{12\mu_L} \delta p_{clo} \tag{7}$$

where Q_{dis} is the distributor flow rate, L_{dis} is the distributor width (z direction), H_{gap} the gap between the distributor and receiver casing, μ_L the dynamic viscosity and $\delta p_{clo} = p_{pump} - p_{receiver}$ is the pressure loss inside the distributor, i.e. the pressure difference between the pump outlet and the receiver, assuming that the pressure losses upstream and downstream from the distributor are neglected.

When the distributor is opened, the singular pressure drop is:

$$\delta p_{ope} = \frac{\rho_L}{2} \left(\frac{Q_{dis}}{L_{dis} \sqrt{H_{gap}^2 + X_{ope}^2}} \right)^2 \tag{8}$$

with $\delta p_{ope} = p_{pump} - p_{receiver}$.

The total pressure drop δp is equal to:

$$\delta p = \delta p_{clo} + \delta p_{ope} \tag{9}$$

Equations (7), (8) and (9) result in the following expression:

$$\frac{1}{2\left(H_{gap}^2 + X_{ope}^2\right)} \left(\frac{Q_{dis}}{L_{dis}} \right)^2 + \frac{12\mu_L X_{clo}}{\rho_L H_{gap}^3} \frac{Q_{dis}}{L_{dis}} - \frac{\delta p}{\rho_L} = 0 \tag{10}$$

Equation (10) shows that the pressure losses are similar in the different distributors and depend only on the engine characteristics.

2.3 Hydraulic system and governing equations

Figure 3 presents the oil hydraulic system previously investigated in [14]: the system is made of a tank, a pump, a rotating distributor, and a piston. During the distributor's opening, the fluid delivered by the pump enters the piston chamber (as illustrated in Fig. 3a and d). During the distributor's closing, the fluid is delivered to an oil tank (Fig. 3e). In the present study, the tank, pump and piston are considered as secondary parts, therefore providing the closure equations for the problem.

Cavitation is generated in the chamber close to the distributor, due to the local pressure drop, as shown in Fig. 3c and d. It is observed at the beginning of the distributor opening, when the gap between the distributor and the chamber is very narrow, thus generating a large pressure drop. The present study is focused on these specific flow conditions. It is assumed that the pressure in the chamber is uniform, so it can be derived from the pressure drop in the gap between the distributor and the chamber. In this simple configuration, the flow rate is thus directly related to the pressure drop.

The flow in this hydraulic system is governed by the following system of equations:

$$\dot{q}_i = \frac{1}{8\pi} \frac{q_i^2}{R_i^3} - \frac{4\mu_L}{\rho_L} \frac{q_i}{R_i^2} + \frac{4\pi R_i}{\rho_L} \left(p_{g_i} + p_v - p_{ex}(t) \right) - \frac{8\pi T}{\rho_L} - \sum_{j=1, j\neq i}^{N_b} \frac{R_i}{D_{ij}} \dot{q}_j \tag{11}$$

$$\frac{1}{2\left(H_{gap}^2 + X_{ope}^2\right)} \left(\frac{Q_{dis}}{L_{dis}} \right)^2 + \frac{12\mu_L X_{clo}}{\rho_L H_{gap}^3} \frac{Q_{dis}}{L_{dis}} - \frac{\delta p}{\rho_L} = 0 \tag{12}$$

$$Q_{pis} = S_{pis} R_{cra} \omega \sin(\omega t) \tag{13}$$

$$\sum_{i=1}^{N_b} q_i + Q_{dis} - Q_{pis} = 0 \tag{14}$$

where $q_i = 4\pi R_i^2 \dot{R}_i$ is the flow rate at the interface of bubble i, $\dot{q}_i = \frac{\partial q_i}{\partial t} = 4\pi \left(2R_i \dot{R}_i^2 + R_i^2 \ddot{R}_i \right)$, Q_{dis} the distributor flow rate, Q_{pis} the piston flow rate, L_{dis} the distributor width (z direction), H_{gap} the gap between the distributor and the chamber casing, S_{pis} the piston section, R_{cra} the crank shaft radius, H_{hei} the chamber height, $\delta p = p_{pump} - p_c$ the total pressure drop, $p_c = p_{ex}(t)$ the chamber pressure and p_{pump} the pressure at the pump outlet.

2.4 Non-dimension governing equations

To obtain non dimensional equations, the following reference parameters are used: the reference length is the average radius $R_{moy} = \left(\frac{3}{4\pi} V_{moy} \right)^{1/3} = \left(\frac{1}{N_b} \sum_{i=1}^{N_b} R_i^3 \right)^{1/3}$, $V_\Omega = 2\pi\Omega R_{dis}$ is the reference velocity, $\frac{R_{moy}}{V_\Omega}$ is the reference time, $\frac{1}{2}\rho_L V_\Omega^2$ is the reference pressure and $R_{moy}^2 V_\Omega$ is the reference flow rate. Hereafter, the same notation (R_i, q_i, p…) is used to write the equations, but all variables are now dimensionless quantities.

Using these reference quantities, the dimensionless counterpart of Eqs. (11)–(14) can be expressed as:

$$\dot{q}_i = \frac{1}{8\pi} \frac{q_i^2}{R_i^3} - \frac{4}{\mathrm{Re}} \frac{q_i}{R_i^2} + 2\pi R_i \left(p_{g_i} - \sigma - C_p(t) \right) - \frac{8\pi}{We} - \sum_{j=1, j\neq i}^{N_b} \frac{R_i}{D_{ij}} \dot{q}_j \tag{15}$$

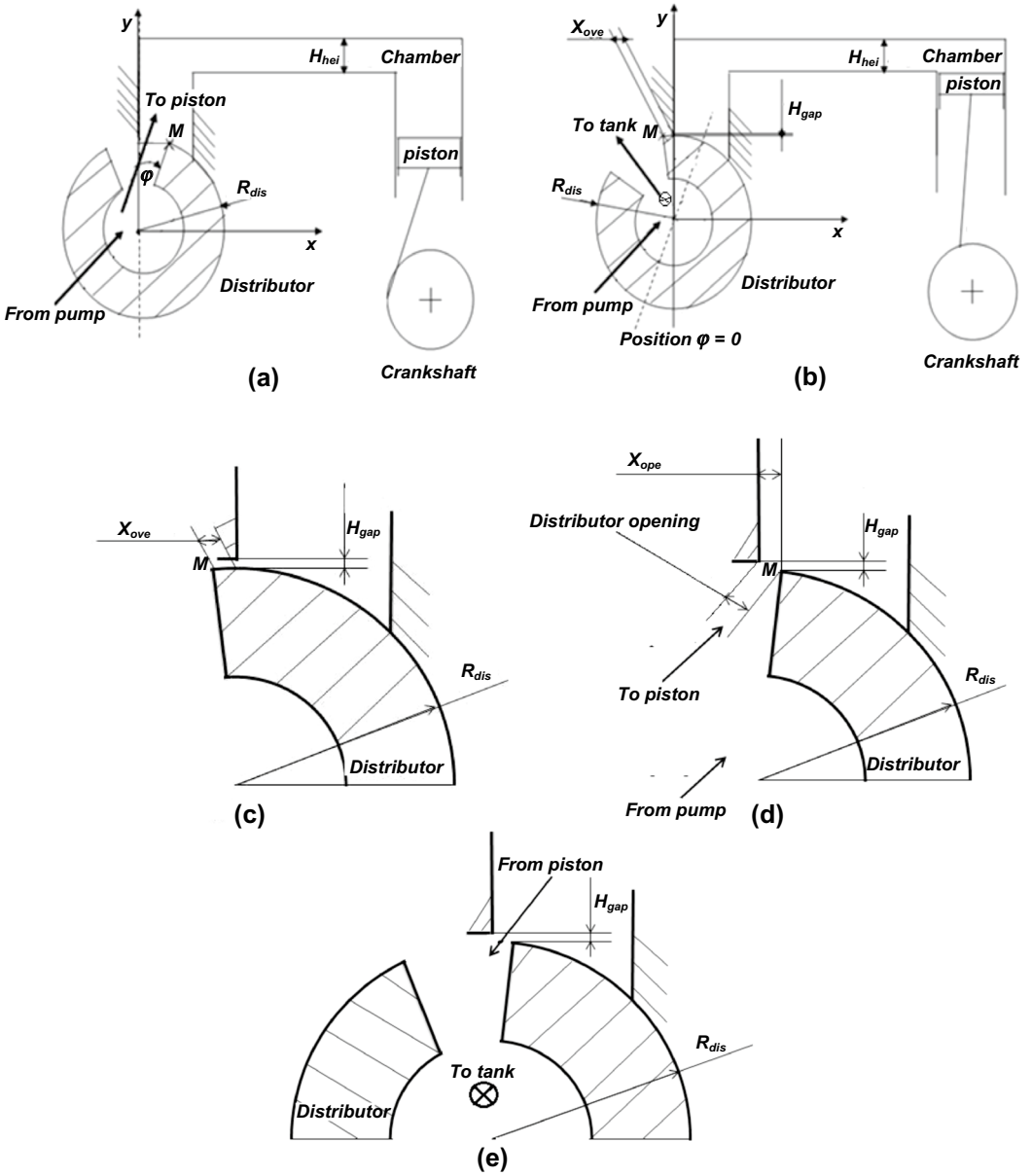

Fig. 3 Scheme of the system **a** distributor opened, **b** distributor closed, **c** and **d** zoom at the overlap in configurations b and a, respectively and **e** zoom at the distributor closing phase

$$\frac{1}{2\left(h_{gap}^2 + X_{ope}^2\right)}\left(\frac{Q_{dis}}{L_{dis}}\right)^2 + \frac{12}{\mathrm{Re}}\frac{X_{clo}}{L_{dis}h_{gap}^3}Q_{dis} - \frac{\delta p}{2} = 0 \quad (16)$$

$$Q_{pis} = S_{pis}R_{cra}\omega\sin(\omega t) \quad (17)$$

$$\sum_{i=1}^{N_b} q_i + Q_{dis} - Q_{pis} = 0 \quad (18)$$

With $\mathrm{Re} = \frac{\rho_L R_{moy} V_\Omega}{\mu_L}$ the Reynolds number, $\mathrm{We} = \frac{\rho_L R_{moy} V_\Omega^2}{T}$ the Weber number, $\sigma = \frac{p_{pump} - p_v}{0.5\rho_L V_\Omega^2}$ the cavitation number, and $C_p(t) = \frac{p_{ex}(t) - p_{pump}}{0.5\rho_L V_\Omega^2}$ the pressure coefficient.

To solve this system of equations, the mass conservation equation provides an equation for the pressure:

$$C_{p_c}^{n+1} = C_{p_c}^{n} + \frac{\varpi}{A_{\Delta p}}\left[\sum_{i=1}^{N_b}\left(\Delta t\dot{q}_i^n + q_i^n\right) + Q_{dis}^n - Q_{pis}^{n+1}\right] \quad (19)$$

With $A_{\Delta p} = 2\pi\Delta t \sum_{i=1}^{N_b} R_i + \frac{1}{2A_{\Delta Q}}$, $A_{\Delta Q} = \left(\frac{|Q_{dis}|}{\left(h_{gap}^2 + X_{ope}^2\right) L_{dis}^2} + \frac{12}{\mathrm{Re}} \frac{X_{clo}}{L_{dis} h_{gap}^3} \right)$ and ϖ a relaxation coefficient.

Further details on the hydraulic system and the numerical method can be found in [14, 16].

2.5 Initial conditions

High precision technology systems use generally clean fluids, i.e. a fluid with a small concentration in nuclei, so a clean fluid is considered in the present study, as in [14]. Experimental measurements of the cavitation nuclei concentration [19] show that very few nuclei smaller than 1 µm are detected, so the initial radius of the smallest bubble is fixed hereafter to $R_{0N_b} = 1$ µm and the biggest one to $R_{01} = 10$ µm. Given the number of bubbles N_b, the radii of the other bubbles are determined by a geometric sequence of common ratio $\left(\frac{R_{0N_b}}{R_{01}}\right)^{\frac{1}{N_b-1}}$: $R_{0i} = \left(\frac{R_{0N_b}}{R_{01}}\right)^{\frac{1}{N_b-1}} R_{0i-1}$, $i \geq 2$. With this distribution, the average radius R_{moy} equals 5.71 µm. The distance between the centers of two bubbles i and j is $D_{ij} = D_0\left(R_{0i} + R_{0j}\right)$ with a given D_0. The initial velocity of the interface $\dot{R}_{0i}$ of bubble i equals zero.

For this application, the HYSPIN AWS 46 oil produced by the BP group is selected. This oil is used for hydraulic systems exposed to high pressure such as power transmission systems and hydraulic jacks. Table 1 provides the oil physical properties and the main geometrical characteristics of the hydraulic system. The resulting cavitation number is σ = 6622.9.

3 Results and discussions

Figure4a and b present the time evolution of the radii of all bubbles for an overlap length $X_{ove} = 2$ and 5 mm, respectively, with the distributor inlet pressure equal to 10 bar, a 12 µm gap, and a rotational speed of 700 rpm. The results show for both values of X_{ove} that only the 6 biggest bubbles (1–6) have developed. However, the lifetime and the bubbles size are much larger for $X_{ove} = 5$ mm (the bubble lifetime is 3.9152 ms for $X_{ove} = 2$ mm vs. 10.6306 ms for $X_{ove} = 5$ mm).

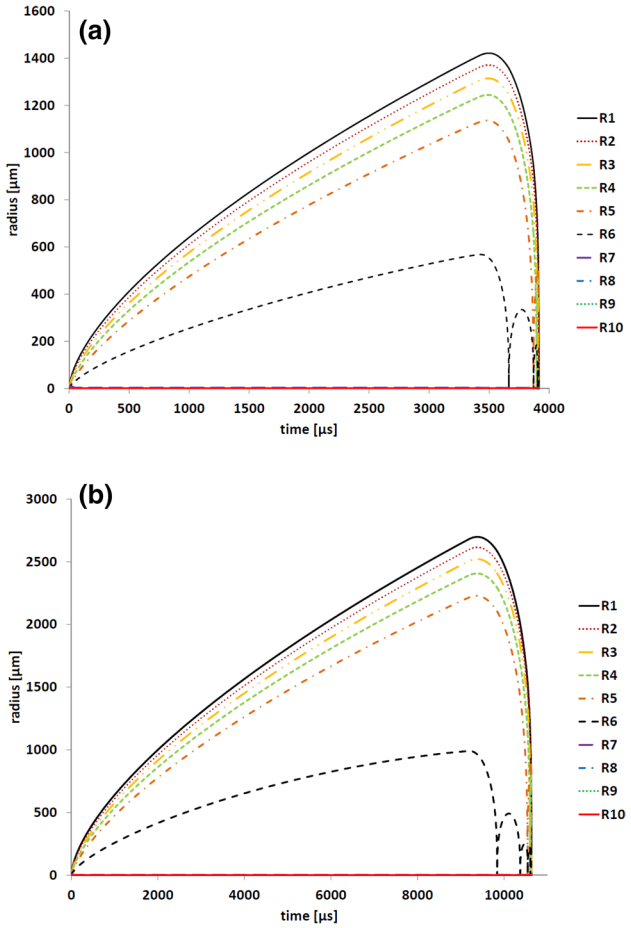

Fig. 4a Time evolution of bubbles radii for $X_{ove} = 2$ mm, $H_{gap} = 12$ µm, Ω = 700 rpm and $p_{pump} = 10$ bar (Re = 63.8, We = 0.06 and σ = 6622.91). Time evolution of bubbles radii for $X_{ove} = 5$ mm, $H_{gap} = 12$ µm, Ω = 700 rpm and $p_{pump} = 10$ bar (Re = 63.8, We = 0.06 and σ = 6622.91)

Figure 5 compares the time evolution of the chamber pressure for $X_{ove} = 2$ and 5 mm. A zoom at the first moments of cavitation shows that the lowest pressure, which corresponds to the bubble nucleation phase, is the same in both cases. It explains why the same number of bubbles develops in both cases (6 bubbles). After the nucleation phase, the bubbles continue to grow while the chamber pressure remains very low. The larger the overlap length, the larger the duration of the distributor opening

Table 1 Characteristics of the oil and geometrical parameters of the system

Density at 40 °C	876 kg/m^3	Gap length	1210^{-6} m
Kinematic viscosity in 40°	4.610^{-5} m^2/s	Distributor radius	810^{-3} m
Surface tension at temperature T = 40°	0.029 N/m	Chamber height	510^{-3} m
Vapor pressure	2400 pa	Crossing area length	210^{-2} m
Pressure at the pump outlet	10^6 pa	Piston area	610^{-5} m^2
Overlap length	10^{-3} m	Crankshaft radius	2.510^{-2} m

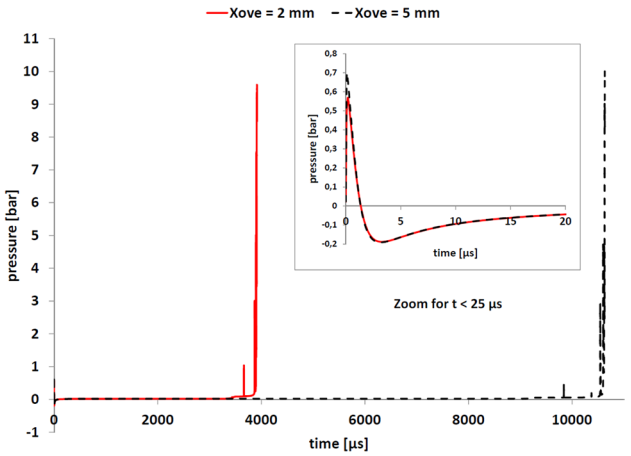

Fig. 5 Time evolution of the chamber pressure for $H_{gap} = 12$ µm, $\Omega = 700$ rpm, $p_{pump} = 10$ bar and $X_{ove} = 2$ and 5 mm (Re = 63.8, We = 0.06 and $\sigma = 6622.91$)

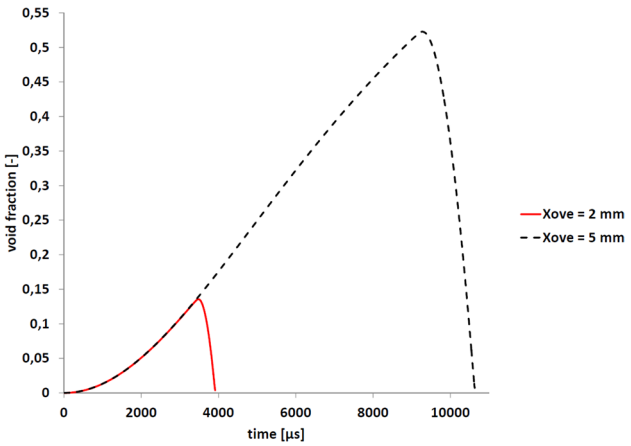

Fig. 6 Time evolution of the void fraction for $H_{gap} = 12$ µm, $\Omega = 700$ rpm, $p_{pump} = 10$ bar and $X_{ove} = 2$ and 5 mm (Re = 63.8, We = 0.06 and $\sigma = 6622.91$)

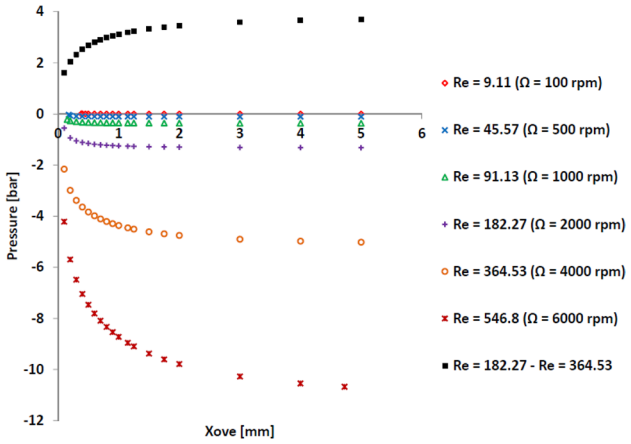

Fig. 7 Evolution of the minimum pressure in the chamber according to X_{ove} for different values of the Reynolds number (rotation speed Ω indicated in parenthesis), $H_{gap} = 12$ µm, $p_{pump} = 10$ bar

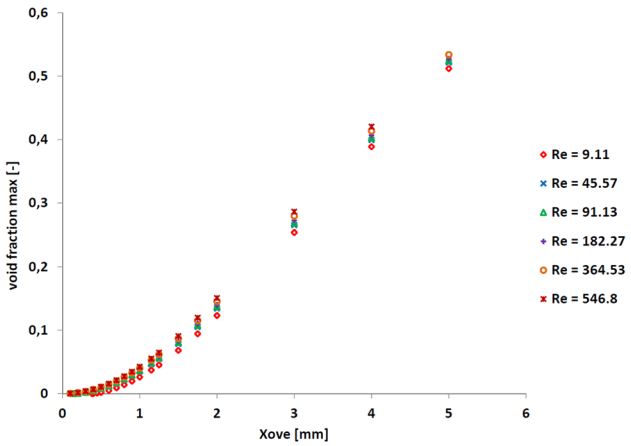

Fig. 8 Maximum void fraction according to X_{ove} for different values of Reynolds number, $H_{gap} = 12$ µm and $p_{pump} = 10$ bar

and thus the longer the duration of this low constant pressure. Therefore, the maximum diameter of the bubbles is significantly larger for $X_{ove} = 5$ mm, compared with $X_{ove} = 2$ mm.

The influence of the overlap length on the cavitation development can be observed in Fig. 6, which compares the time evolution of the void fraction for $X_{ove} = 2$ and 5 mm. The void fraction is the ratio between the total volume of the bubbles and the chamber volume V_{ch}. It provides a global vision of the cavitation development. The results show that the maximum void fraction for $X_{ove} = 5$ mm is almost 4 times higher than the one obtained for $X_{ove} = 2$ mm.

Figure 7 presents the minimum pressure in the chamber as a function of the overlap length for different values of the rotation speed, i.e. different values of the Reynolds number values. In addition, it shows the difference between the curves obtained at 2000 and 4000 rpm (Re = 182.27 and Re = 364.53, respectively). The results show that both the rotational speed and the overlap length strongly influence the pressure drop: increasing the overlap length and/or the rotational speed significantly amplifies the pressure drop.

The difference between the two curves Re = 182.27 and Re = 364.53 is also drawn.

Indeed, for a given overlap length, the results show that the minimum pressure decreases when the rotational speed increases, so the number of growing bubbles should increase and it is expected that the void fraction

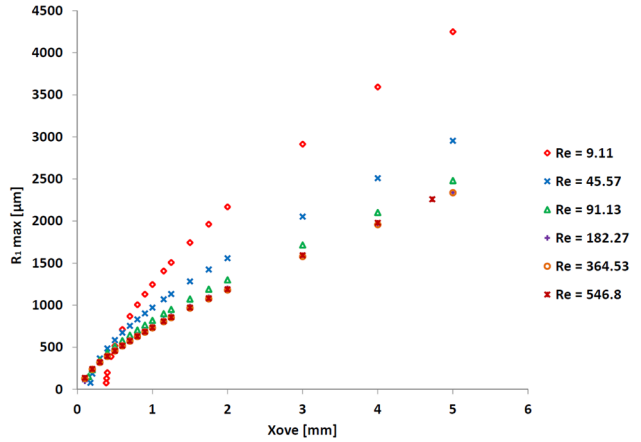

Fig. 9 Maximum radius R_1 according to X_{ove} for different values of Reynolds number Re $H_{gap} = 12$ µm and $p_{pump} = 10$ bar

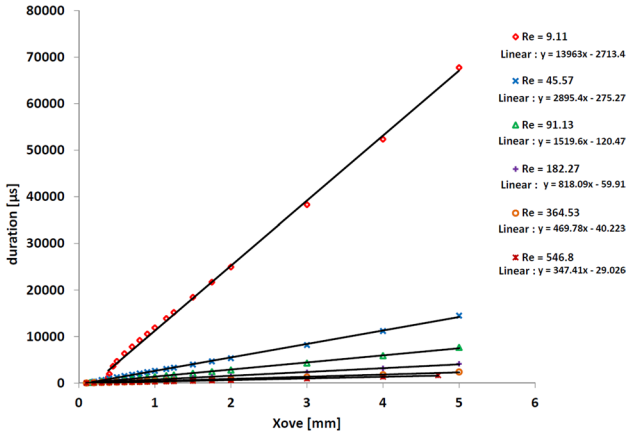

Fig. 10 Cavitation duration with respect to X_{ove} for different values of the Reynolds number $H_{gap} = 12$ µm and $p_{pump} = 10$ bar

should, in turn, increase significantly. However, as shown in Fig. 8, which displays the maximum void fraction as a function of the overlap length for different values of rotation speed, there is almost no difference between the curves obtained at different rotation speeds. The results show that even at low rotational speed, i.e. with a low pressure drop and a small number of bubbles that develop, the void fraction is nearly identical to the one obtained at high speed, although the pressure drop is much higher, and more bubbles develop.

Indeed, as showed previously [14], the growth of more bubbles induces more interactions between these bubbles, which eventually slows down the development of the bubbles. To check this effect, Fig. 9 displays the maximum radius of the biggest bubble as a function of the overlap length for different rotation speeds. For a given overlap length, the more the rotation speed decreases, the more the maximum radius of the biggest bubble increases. This difference in the bubble development explains why the rotation speeds have very little influence on the global void fraction.

Most importantly, the results show that the overlap length has a preponderant influence on the cavitation development, compared with the rotation speed, which confirms that a modelling of the effect the overlap length is needed to avoid or minimize the development of cavitation.

Figure 10 presents the cavitation duration as a function of the overlap length for different rotation speeds. It can be observed that for all rotational speeds, i.e. all values of the Reynolds number, the cavitation duration is proportional to the overlap length, but with different slopes. Thus, for a given rotation speed, the extrapolation of the linear curve enables to determine the value X_{ove} corresponding to a zero-cavitation duration, i.e. the overlap

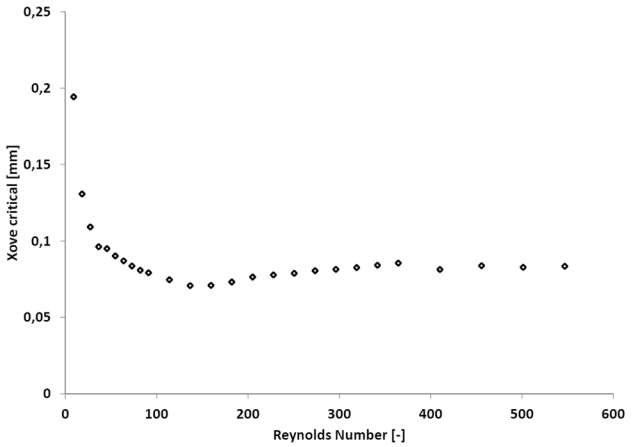

Fig. 11 Critical value of X_{ove} according to the Reynolds number $H_{gap} = 12$ µm and $p_{pump} = 10$ bar

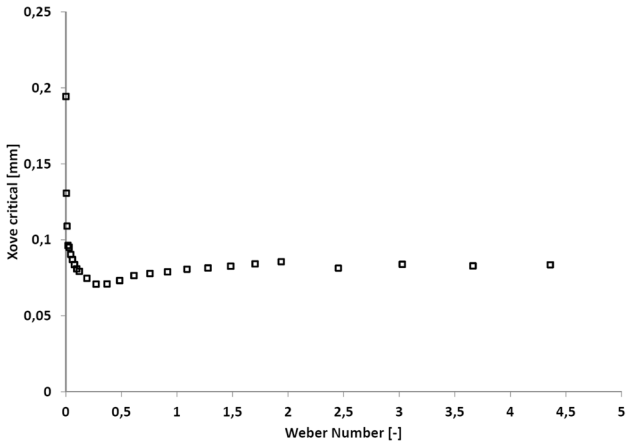

Fig. 12 Critical value of X_{ove} according to the Weber number $H_{gap} = 12$ µm and $p_{pump} = 10$ bar

length where no bubble has a sufficient time to develop. This specific overlap length can thus be considered as the maximum appropriate overlap to avoid cavitation (the critical overlap length).

Figures 11 and 12 present the Reynolds and Weber number as a function of the critical overlap length, respectively. It can be seen that the two curves are similar. The Reynolds and Weber numbers are strongly dependent on the same parameters, namely the average radius R_{moy} and the rotational speed, so only the Reynolds number curve is analyzed hereafter.

The results show that when the Reynolds number tends to zero, the critical overlap length tends asymptotically to infinity. Small Reynolds numbers correspond to a rotational speed or an average radius R_{moy} close to zero.

In the first case, it means that the distributor is almost in the closed position, When the distributor is closed, for any value of the overlap length, the oil can flow through the gap between the distributor and the chamber casing. The previous study [14] shows that for any value of the gap within a typical range, no significant cavitation development is obtained.

The second case implies that almost no cavitation nucleus is present in the liquid. Experimental studies show that such a pure liquid can experience large negative pressure without cavitation [20, 21]: so if the oil is very pure, i.e. very clean, a very intense pressure drop is required to initiate cavitation. So, for a rotational speed or an average radius R_{moy} close to zero, it is extremely difficult to create cavitation, whatever the value of the overlap length. The critical length thus tends to infinity.

When the Reynolds number tends to infinity, it means that the rotation speed tends to infinity, since the average radius R_{moy} is necessarily restricted in a liquid. In that case the critical overlap length tends asymptotically to 0.084 mm. In between the two asymptotes, the curve exhibits a global minimum and a local maximum of 0.071 and 0.086 mm, respectively. So, the 0.071 mm value is found to be the critical length of the hydraulic distributor at cavitation inception, even in the case of a variable speed.

4 Conclusion

The present study is an extension of the previous work reported in [14], where the existence of a critical length of the overlap was demonstrated: for values higher than this limit, the cavitation duration and the maximum void fraction are significantly influenced. In the present work, a modelling of the critical overlap length of hydraulic distributors at cavitation inception was conducted.

The study shows that the pressure losses in a rotating distributor and in a slide-valve, which are used in most of the cases in hydraulic systems, can be expressed similarly, so a single study can be conducted to analyze the effects of the overlap length.

It was also shown that different values of the rotation speed can lead to nearly identical void fraction evolutions. However, when the rotation speed is decreased, the pressure drop also decreases, and less cavitation bubbles are growing, so it was expected that the void fraction would decrease. But when less bubbles develop, less interactions between bubbles are obtained, so the bubbles reach a larger diameter. This difference in the development of the bubbles explains why the rotation speed has almost no influence on the void fraction.

In addition, it was found that increasing the overlap length also increases the duration of the distributor opening and the period of low pressure in the chamber, which in turns promotes the expansion of the cavitation bubbles. So, the increase of the overlap length results in bigger cavitation bubbles, and eventually a higher void fraction.

Most important is the observation that a small geometrical detail like the overlap length has a large influence on the cavitation development, even larger than the rotation speed. A critical overlap length of 0.071 mm was obtained for the specific distributor studied here, below which no significant cavitation development is obtained, for any rotation speed. A possible improvement of the current study, in future works, would be to take into account some non-uniform pressure in the chamber, which could induce some pressure gradients and convection of cavitation bubbles. This effect was non considered in the present work.

Declaration

Conflict of interest The authors declare that they have no conflict of interest.

References

1. Liao Y, Martins JR, Young YL (2021) 3-D high-fidelity hydrostructural optimization of cavitation-free composite lifting surfaces. Compos Struct 268:113937
2. Izadyar H, Aghababaei A, Forghani P, Hajighasemi A (2020) Investigation of rib's effect in cavitation on an axisymmetric separated flow over a longitudinal blunt circular cylinder. SN Applied Sciences 2:588
3. Silva PASF, Shinomiya LD, de Oliveira TF, Vaz JRP, Mesquita ALA, Junior ACPB (2017) Analysis of cavitation for the optimized design of hydrokinetic turbines using BEM. Appl Energy 185(2):1281–1291
4. Shafaghat R, Hosseinalipour SM, Lashgari I, Vahedgermi A (2011) Shape optimization of axisymmetric cavitators in supercavitating flows, using the NSGA II algorithm. Appl Ocean Res 33(3):193–198
5. Lin C-C, Lee Y-J, Hung C-S (2009) Optimization and experiment of composite marine propellers. Compos Struct 89(2):206–215
6. Blasques JP, Berggreen C, Andersen P (2010) Hydro-elastic analysis and optimization of a composite marine propeller. Mar Struct 23(1):22–38
7. Khaled M, Gad El Rab M, Hachem F, Elhage H, Elmarakbi A, Harambat F, Peerhossaini H (2016) Experimental study of the flow induced by a vehicle fan and the effect of engine blockage in a simplified model. Int J Automot Technol 17(4):617–627
8. Singh P, Nestmann F (2009) Experimental optimization of a free vortex propeller runner for micro hydro application. Exp Thermal Fluid Sci 33(6):991–1002
9. Deshmukh PA, Deshmukh KD, Mandhare NA (2020) Performance enhancement of centrifugal pump by minimizing casing losses using coating. SN Appl Sci 2:252
10. Sun ZC, Mao YF, Fan MH (2020) Performance optimization and investigation of flow phenomena on tidal turbine blade airfoil considering cavitation and roughness. Appl Ocean Res 106:102463
11. Bertetta D, Brizzolara S, Gaggero S, Viviani M, Savio L (2012) CPP propeller cavitation and noise optimization at different pitches with panel code and validation by cavitation tunnel measurements. Ocean Eng 53:177–195
12. Lee MG, Lim CS, Han SH (2016) Shape design of the bottom plug used in a 3-way reversing valve to minimize the cavitation effect. Int J Precis Eng Manuf 17(3):401–406
13. Talha A, Barrand JP, Neyrat S, Aubret P, Jonquet D (2001) Etude expérimentale de réduction du bruit d'une pompe à engrenages de boîte de vitesses automatique. Méc Ind 2(2):149–156
14. Adama Maiga M, Coutier-Delgosha O, Buisine D (2015) Cavitation in a hydraulic system: the influence of the distributor geometry on cavitation inception and study of the interactions between bubbles. Int J Engine Res 8(4):183–213
15. Ohl CD (2002) Cavitation inception following shock wave passage. Phys Fluid 14(10):3512–3521
16. Adama Maiga M, Coutier-Delgosha O, Buisine D (2018) Analysis of the critical pressure of cavitation bubbles. Meccanica 53(4):787–801
17. Bremond N, Arora M, Dammer SM, Lohse D (2006) Interaction of cavitation bubbles on a well. Phys Fluids 18:1215505
18. Ida M (2009) Multibubble cavitation inception. Phys Fluids 21:113302
19. Franc J-P, Kueny J-L, Karimi A, Fruman D-H, Fréchou D, Briançon-Marjollet L, Billard J-Y, Belahadji B, Avellan F, Michel J-M (1995) La cavitation: Mécanismes physiques et aspects industriels. EDP Sciences-Collection, Grenoble Sciences p 55
20. Briggs LJ (1950) Limiting negative pressure in water. J Appl Phys 21:721–722
21. Zheng Q, Durben DJ, Wolf GH, Angell CA (1991) Liquids at large negative pressures: water at the homogeneous nucleation limit. Science 254:829–832